



Research paper

Hydrothermal synthesis of chlorite from saponite: Mechanisms of smectite-chlorite conversion and influence of Mg^{2+} and Al^{3+} suppliesPan Liu^{a,1}, Wei Kai^a, Chen Zhu^a, Yuanzhi Tang^b, Wancang Zhao^{a,*,2}, Yuanfeng Cai^c, Jingong Cai^d, Junfeng Ji^a^a Key Laboratory of Surficial Geochemistry, School of Earth Sciences and Engineering, Ministry of Education, Nanjing University, Nanjing 210046, China^b School of Earth and Atmospheric Sciences, Georgia Institute of Technology, Atlanta 30332, USA^c State Key Laboratory for Mineral Deposits Research, School of Earth Science and Engineering, Nanjing University, Nanjing 210046, China^d State Key Laboratory of Marine Geology, Tongji University, Shanghai 200092, China

ARTICLE INFO

Keywords:

Smectite-chlorite conversion

Hydrothermal synthesis

Solid state transformation

Polymerization

Al substitution

ABSTRACT

Conversion of smectite to chlorite (S–C conversion) is a common clay transformation reaction in a range of geological settings. Yet, current models for S–C conversion are still under debate. This study systematically investigated the mechanisms of S–C conversion and the influences of Mg^{2+} and Al^{3+} supplies. Saponite (a representative trioctahedral smectite) was reacted with Mg^{2+} and Al^{3+} under 340 °C and autogenous pressure. Reaction was found to reach steady state around 24 h, and either randomly mixed-layered chlorite/smectite (C/S) or chlorite formed from saponite. Solution chemistry and mineralogical evidence suggested that the S–C conversion occurred through solid-state transformation, characterized with gradual formation of hydroxide layers from Mg–Al polymers via polymerization in interlayer and concomitant substitution of Al for Si in 2:1 layers. The formation of mixed-layered C/S or chlorite depended on Mg^{2+} and Al^{3+} supplies. When Mg^{2+} and Al^{3+} were limited, mixed-layered C/S would form from saponite, and growing Mg^{2+} and Al^{3+} supplies would continuously increase the percentage of chlorite in mixed-layered C/S until chlorite formed (saponite → mixed-layered C/S → chlorite). In contrast, chlorite could form directly from saponite under sufficient Mg^{2+} and Al^{3+} supplies (saponite → chlorite). This study contributed to an improved understanding of S–C conversion, and provided a general methodology and knowledge basis for future studies involving this mineral conversion.

1. Introduction

The conversion of trioctahedral smectite (e.g., saponite) to chlorite is by far the most common transformation of trioctahedral clay minerals (Beaufort et al., 2015), occurring in a wide range of geological settings, such as diagenetic systems (e.g., April, 1981; Chang et al., 1986), low-grade metamorphic systems (e.g., Bettison and Schiffman, 1988; Inoue and Utada, 1991; Shau et al., 1990), hydrothermal systems (e.g., Robinson and De Zamora, 1999; Schiffman and Staudigel, 1995), and subduction zones (e.g., Schleicher et al., 2012). An in-depth understanding of the mechanisms of smectite-to-chlorite (S–C) conversion is critical for accurate application of chlorite as a geothermometer to reconstruct thermal histories of basins and hydrothermal systems (Beaufort et al., 2015), for better predictions of petroleum formation process and reservoir quality associated with chlorite (Dowey et al.,

2012), and for understanding the roles of clay transformations in faulting processes (Meng et al., 2018).

Despite the above mentioned significances, the kinetics and mechanisms of S–C conversion is still under debate (reviewed in Beaufort et al., 2015; Robinson et al., 2002). Three contrasting models have been proposed based on field observation: (1) a continuous model, which accommodates the transformation from smectite to randomly mixed-layered chlorite/smectite (C/S), followed by chlorite (e.g., Chang et al., 1986); (2) a discontinuous model, which is characterized with the occurrence of corrensite (regularly mixed-layered C/S) but in absence of randomly mixed-layered C/S (e.g., Inoue and Utada, 1991; Shau and Peacor, 1992); and (3) a direct model with direct transformation of saponite to chlorite with no occurrence or only minor occurrence of C/S (Robinson et al., 2002). In addition, a wide range of factors (such as temperature, bulk-rock composition/mineralogy, fluid/rock ratio, etc)

* Corresponding author.

E-mail addresses: wancangzhao@nju.edu.cn, geodoer@swu.edu.cn (W. Zhao).¹ Present address: School of Earth and Atmospheric Sciences, Georgia Institute of Technology, Atlanta 30332, USA.² Present address: Chongqing Key Laboratory of Karst Environment, School of Geographical Sciences, Southwest University, Chongqing 400715, China.

Table 1
Summary of hydrothermal experiments conducted in this study.

Series	Al ³⁺ (mM)	Mg ²⁺ (mM)	Mg/Al molar ratio	Time	Sample labels	Notes	Products	
I	85	185	2.2	0–72 h	I-reaction time	Reaction kinetics	Chlorite	
II	135	170	1.3		II-reaction time		Chlorite & boehmite	
III	185	135	0.7		III-reaction time		Chlorite & boehmite	
IV	8	18	2.2	24 h	IV-A1	Increasing Mg ²⁺ and Al ³⁺ initial supplies	C/S (10%C) ^a	
	16	36	2.2		IV-A2		C/S (21%C)	
	24	54	2.2		IV-A3		C/S (40%C)	
	32	72	2.2		IV-A4		C/S (48%C)	
	40	90	2.2		IV-A5		C/S (62%C)	
	48	108	2.2		IV-A6		C/S (70%C)	
	56	126	2.2		IV-A7		C/S (75%C)	
	64	144	2.2		IV-A8		C/S (80%C)	
	72	162	2.2		IV-A9		C/S (84%C)	
	100	180	1.8		IV-B1	Increasing Al ³⁺ but decreasing Mg ²⁺ initial supplies	Chlorite	
	120	170	1.4		IV-B2		Chlorite & boehmite	
	135	160	1.2		IV-B3		Chlorite & boehmite	
	170	145	0.9		IV-B4		Chlorite & boehmite	
	220	120	0.5		IV-B5		Chlorite & boehmite	
	0	0	–		IV-C1		Blank	C/S (3%C)
	0	185	–		IV-C2		Al-free control	C/S (20%C)
	185	0	–		IV-C3		Mg-free control	Multiple phases

For all series, solution (mL)/saponite (g) = 30, initial pH within 9.0 ± 0.1, and experimental temperature at 340 °C.

^a Randomly mixed-layered chlorite/smectite with percentage of chlorite in parentheses. The percentage of chlorite was determined by the (001) reflection position after ethylene glycol solvation (Reynolds, 1980).

may influence the conversion, but the effects of each factor are not clear as well.

To better understand the mechanisms and pathways of S–C conversion, hydrothermal synthesis of chlorite under controlled conditions has been employed. For example, transformation from saponite to corrensite without occurrence of randomly mixed-layered C/S was observed in hydrothermal reaction at 350 °C for 22 d or at 500 °C for 6 h (Roberson et al., 1999). Chlorite and mixed-layered minerals (e.g., chlorite/vermiculite/saponite) have been synthesized using montmorillonite or vermiculite as precursor (Meng et al., 2018; Mosser-Ruck et al., 2010; Mosser-Ruck et al., 2003). In a long term experiment (9 years), the conversion of montmorillonite to chlorite was proposed to take place via several steps involving the formation of mixed-layered C/S and corrensite/chlorite (Mosser-Ruck et al., 2016).

Despite the previous experimental efforts, S–C conversion is still not fully understood, because most previous studies used dioctahedral smectite (such as montmorillonite) (e.g., Meng et al., 2018) rather than trioctahedral smectite (such as saponite) as precursor. However, trioctahedral smectite is the most common precursor of S–C conversion observed in the fields (Beaufort et al., 2015). Additionally, those studies focused on smectite stability in contact with Fe metal in nuclear waste repository, which resulted in the formation of Fe-rich saponite and Fe-chlorite (e.g., Guillaume et al., 2003; Mosser-Ruck et al., 2010). However, most chlorite in shallow hydrothermal and diagenetic systems has an Fe/(Fe + Mg) ratio of < 0.5 (Beaufort et al., 2015). Thus, studies on the conversion of Mg-rich saponite to Mg-chlorite are highly desired towards better understandings of S–C conversion in hydrothermal and diagenetic systems.

In this study, we systematically investigated the mechanisms of S–C conversion. Saponite (a representative trioctahedral smectite) was reacted with Mg²⁺ and Al³⁺ in NaCl solution at 340 °C, autogenous pressure (14.5 bar), liquid/solid ratio of 30, and initial pH of 9.0 for up to 72 h. A suit of complementary techniques was employed to characterize the composition, morphology, and structure of the reaction products, including inductively coupled plasma optical emission spectrometry (ICP-OES), X-ray diffraction (XRD), thermogravimetric analysis and differential scanning calorimetry (TGA-DSC), scanning electron microscopy coupled with energy dispersive X-ray spectroscopy (SEM-EDX), transmission electron microscopy (TEM), Fourier transform infrared spectroscopy (FTIR), and nuclear magnetic resonance (NMR) spectroscopy. The results revealed detailed mechanisms of S–C

conversion and roles of Mg²⁺ and Al³⁺ supplies in determining S–C conversion pathways, and provided a general methodology and knowledge basis for future studies on this mineral conversion.

2. Experimental procedure

2.1. Saponite preparation

All chemicals used for experiments were analytical grade or higher. Saponite was synthesized according to well-established method (He et al., 2014). Specifically, 27 g NaOH, 49.2 g NaHCO₃, and 72.8 g Na₂SiO₃·9H₂O were dissolved in 350 mL deionized (DI) water to obtain solution A. Solution B was prepared by dissolving 11.5 g AlCl₃·6H₂O and 46.2 g MgCl₂·6H₂O in 50 mL DI water. Then, solution B was slowly added to solution A under vigorous stirring for 15 min. The mixture was then heated at 180 °C and autogenous pressure in a hydrothermal reactor (Parr Instruments) for 24 h. At the end of reaction, solid products were collected by vacuum filtration, rinsed by 2 L DI water, dried at 60 °C, and finely ground for further characterization. The successful synthesis of saponite was confirmed by XRD and other analytic techniques and discussed later.

2.2. Hydrothermal synthesis of chlorite from saponite

0.5 g saponite was added to 15 mL 0.05 M NaCl solution (liquid/solid ratio = 30 mL/g), which contained different concentrations of MgCl₂ and AlCl₃. Saponite was dispersed in solution by stirring for 2 h, during which pH of the suspension was slowly titrated to pH 9.0 using NaOH solution. The suspension was transferred into hydrothermal reactors and heated at 340 °C and autogenous pressure. After pre-determined reaction time, reactors were quenched to room temperature. Then, the reacted suspension was transformed into 50 mL centrifuge tubes, and pH was measured at room temperature. The solution phase and solid products were separated by centrifugation at 5000 rpm for 10 min. Cation concentrations of the solution were measured by ICP-OES (see Section 2.3.1). The solid products were further rinsed by DI water and dried at 60 °C. About 0.7 g solid products were yielded for each experiment.

Overall, four series of experiments were conducted (Table 1). Series I, II, and III aimed to study the kinetics of S–C conversion with different Mg/Al ratios. Hydrothermal reactors were quenched to room

temperature after different time intervals (0.08–72 h). Series IV with 17 experiments aimed to investigate the effects of Mg^{2+} and Al^{3+} supplies on S–C conversion: IV-A1 to IV-A2 had increasing Mg^{2+} and Al^{3+} supplies but with a constant Mg/Al ratio; IV-B1 to IV-B5 were characterized with decreasing Mg/Al ratios; and IV-C1, IV-C2, and IV-C3 were control experiments. Reactors in Series IV were quenched to room temperature at 24 h based on the kinetics of Series I–III (see Section 3.2).

2.3. Characterization of reaction products

2.3.1. Solution characterization

Cation concentrations (Mg, Al, and Fe) in solution phase were measured by ICP-OES using iCAP 6500 DUO (Thermo Fisher Scientific). Fe concentration was monitored during reaction because of concern on reactor corrosion during reaction. Solution was filtrated, diluted, and acidified to 2% HNO_3 (vol%) prior to measurement. A series of calibration standards with known concentrations (0–500 ppm) was prepared using certified standard solution (TraceCERT). Calibration standards were measured every 10 samples to ensure accuracy.

2.3.2. Solid characterization

2.3.2.1. Cation exchange capacity (CEC). CEC of the saponite and solid products was obtained following standard procedures (Chapman, 1965). Briefly, about 100 mg sample was dispersed in 10 mL of 1 M ammonium acetate ($NH_4CH_3CO_2$, pH 7.0) and stirred overnight to reach cation exchange equilibrium, followed by centrifugation at 5000 rpm for 10 min to separate the solids and supernatant. Cation exchange was repeated for three times, and the accumulative supernatant was prepared for ICP-OES measurement with the same procedure as mentioned above (see Section 2.3.1). The main cations detected in the supernatant were Na^+ and Mg^{2+} .

2.3.2.2. X-ray diffraction (XRD). Oriented XRD patterns were recorded on a Rigaku D/max IIIa diffractometer ($Cu K\alpha$, $\lambda = 0.154$ nm) at 40 kV and 40 mA. Oriented samples after different treatments, including air-dried (AD), ethylene glycol-solvated (EG), Mg^{2+} -saturated (Mg^{2+}), and heated at 350 or 550 °C for 2 h (H-350 or H-550), were scanned from 2 to 40°2 θ with a step of 0.01°2 θ and a rate of 1°2 θ /min. The percentage of chlorite (%C) in mixed-layered C/S was estimated based on the (001) reflection position after EG solvation (Reynolds, 1980).

2.3.2.3. Scanning electron microscopy coupled with energy dispersive X-ray spectroscopy (SEM-EDX). Solid samples were first dusted on carbon tapes and coated with platinum. SEM imaging (Carl Zeiss Supra 55) was performed at 5 kV and 10 μA with a working distance of 5 mm. As for chemical analysis, EDX spectra were collected at 15 kV and 30 μA with a working distance of 15 mm using Oxford Aztec X-Max 150. Each spectra were collected for > 1 min to get higher signal/noise ratios. For each sample, 6–15 spectra were collected for each mineral phase

Table 2

Chemical formulae of saponite and chlorite based on EDX analysis.

Sample	Al^{3+} (mM)	Mg^{2+} (mM)	Na	Mg	^{IV}Al	^{VI}Al	Si	Fe
Saponite	/	/	0.57 (0.10)	2.86 (0.23)	0.58 (0.13)	0.09 (0.14)	3.42 (0.13)	0.02 (0.02)
I-24h	85	185	0.02 (0.03)	4.96 (0.10)	0.84 (0.07)	0.89 (0.04)	3.16 (0.07)	0.11 (0.03)
IV-B1	100	180	0.00 (0.00)	4.85 (0.06)	0.93 (0.04)	1.01 (0.03)	3.07 (0.04)	0.09 (0.02)
IV-B2	120	170	0.01 (0.02)	4.72 (0.06)	1.01 (0.02)	1.12 (0.04)	2.99 (0.02)	0.11 (0.01)
II-24h	135	170	0.01 (0.03)	4.65 (0.08)	1.04 (0.05)	1.15 (0.06)	2.96 (0.05)	0.14 (0.02)
IV-B3	135	160	0.01 (0.02)	4.46 (0.06)	1.00 (0.07)	1.26 (0.05)	3.00 (0.07)	0.15 (0.03)
IV-B4	170	145	0.00 (0.01)	4.23 (0.09)	1.11 (0.07)	1.44 (0.08)	2.89 (0.07)	0.16 (0.02)
III-24h	185	135	0.00 (0.00)	4.03 (0.17)	1.13 (0.12)	1.50 (0.14)	2.87 (0.12)	0.29 (0.10)
IV-B5	220	120	0.01 (0.03)	3.98 (0.07)	1.08 (0.04)	1.49 (0.06)	2.92 (0.04)	0.32 (0.03)

Saponite formula was calculated on the scale of $O_{10}(OH)_2$ and chlorite on the scale of $O_{10}(OH)_8$. All Fe in the structure were assumed to be divalent. Numbers in parentheses represent standard deviation.

identified (e.g., mixed-layered C/S, chlorite, and boehmite, see Section 3.2.2). Averaged element contents of each mineral phase were reported in Table S1 (Supplementary Data).

2.3.2.4. Transmission Electron Microscopy (TEM). Selected samples were ultrasonically dispersed in an ethanol-water solution. One drop of the suspension was placed on a copper grid and dried at room temperature. Samples were coated by carbon, and then examined by FEI Tecnai F20 at 200 kV. TEM analysis included selected area electron diffraction (SAED) (recorded normal to the clay layer) and 00l lattice fringe imaging (parallel to the clay layer).

2.3.2.5. Thermogravimetric analysis and differential scanning calorimetry (TGA-DSC). The simultaneous TGA and DSC analyses were conducted on a thermogravimetric analyzer (TGA/DSC 1, Mettler Toledo), which was calibrated using certified standards before sample measurements. About 10 mg samples were loaded in an alumina pan and heated from room temperature to 1000 °C at a heating rate of 20 °C/min with N_2 flow of 100 mL/min.

2.3.2.6. Fourier transform infrared spectroscopy (FTIR). Selected samples were mixed with KBr at a clay/KBr mass ratio of 1/100 and ground in an agate mortar for > 15 min, after which samples were dried in an oven at 105 °C for 24 h to minimize water adsorption. After drying, samples were packed into a cylindrical cup and FTIR spectra were obtained using a Thermo Nicolet FTIR 6700 spectrometer. All spectra were collected at room temperature over the range of 400–4000 cm^{-1} with a resolution of 4 cm^{-1} . Each sample was scanned 128 times to get optimal spectral quality.

2.3.2.7. Nuclear magnetic resonance spectroscopy (NMR). Solid-state ^{29}Si and ^{27}Al magic angle spinning (MAS) NMR measurements were carried out on a Bruker Avance 400 spectrometer at ^{29}Si resonance frequency of 79.5 MHz and ^{27}Al frequency of 104.3 MHz, respectively. Samples were packed in a 4 mm ZrO_2 rotor. Direct polarization (DP) MAS NMR spectra of ^{29}Si were recorded with an acquisition time of 32 ms and a recycle delay of 4 s at 10 kHz. The ^{29}Si chemical shifts were externally referenced to tetramethylsilane. ^{27}Al DP MAS NMR spectra were collected with an acquisition time of 8 ms and a recycle delay of 4 s at 12 kHz. The ^{27}Al chemical shift was externally referenced to 1.0 M $Al(NO_3)_3$ solution.

3. Results and discussion

3.1. Characteristics of saponite

In order to show the S–C conversion, results of saponite were reported along with solid products in Tables 1–2 and Figs. 1–7. Saponite was characterized with a strong (001) reflection at 12.6 Å (7.0°2 θ) (Moore and Reynolds, 1989) (Fig. 2). As indicated by the position of (001) reflection, saponite expanded to 17.3 Å (5.1°2 θ) as solvated by EG

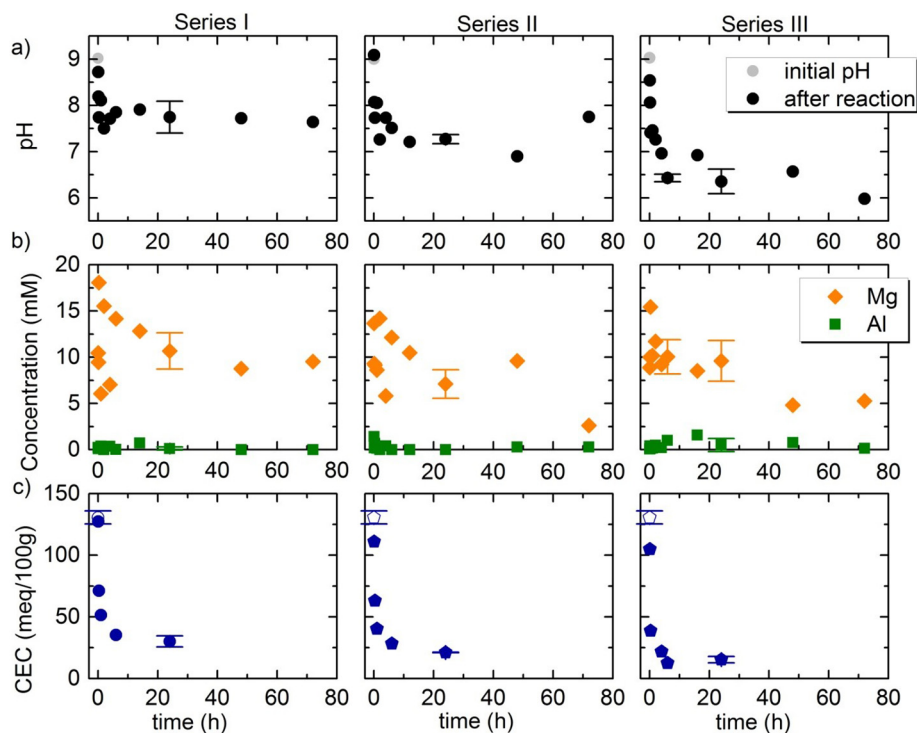


Fig. 1. Evolution of solution phase and solid products during S-C conversion in Series I-III. a) pH and b) Mg and Al concentrations of solution phase; c) CEC of saponite and solid products. In (c), open symbols denote saponite, while solid symbols represent solid products. Error bars were calculated in duplicates.

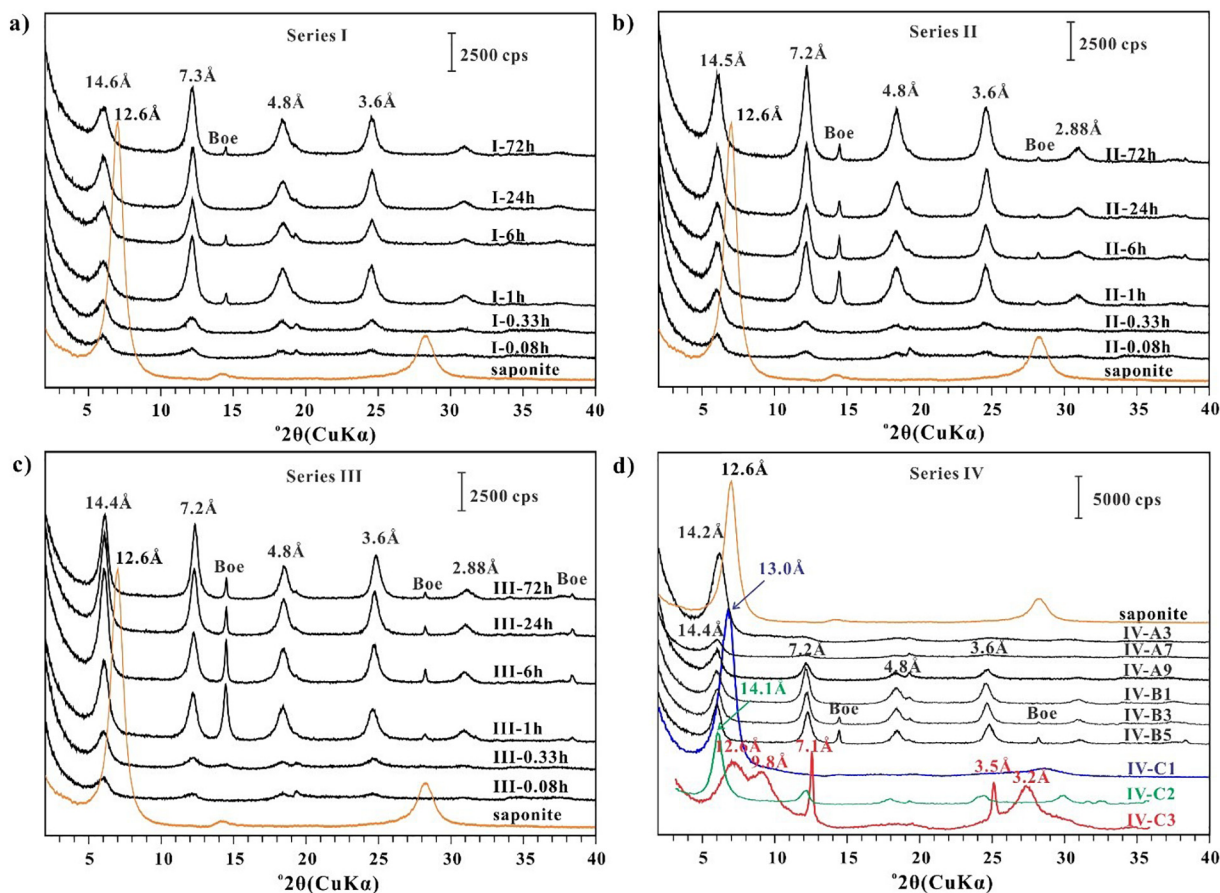


Fig. 2. Oriented XRD patterns of air-dried saponite and solid products from Series I-IV. Boe: boehmite. See Figs. S4 and S5 for more XRD patterns of solid products in Series IV.

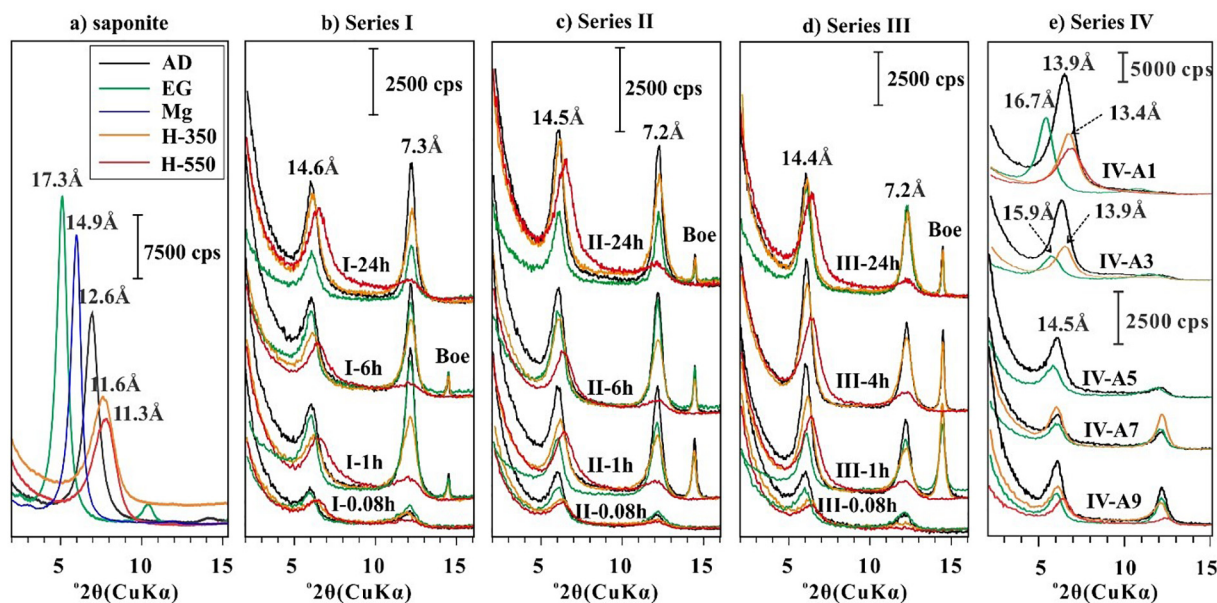


Fig. 3. Oriented XRD patterns of saponite and solid products from Series I–IV after different treatments. AD: air-dried; EG: ethylene glycol-solvated; Mg: Mg^{2+} -saturated; H-350 or H-550: heated at 350 or 550 °C for 2 h; Boe: boehmite. In (e), XRD intensity of IV-A1 and IV-A3 was plotted with scale bar of 5000 cps, while the rest were plotted with scale bar of 2500 cps for visualization. See Figs. S4 and S5 for more XRD patterns of solid products from Series IV.

and collapsed to 11.3 Å ($7.8^\circ 2\theta$) after heat treatment (Fig. 3a). In SEM images, flaky structure of saponite was clearly observed, and there were no other amorphous or crystalline phases (Fig. 4a). Based on EDX results (Table S1), the chemical formula of saponite was $Na_{0.57}(Mg_{2.86}Al_{0.09}Fe_{0.02})(Al_{0.58}Si_{3.42})O_{10}(OH)_2$ on the scale of $O_{10}(OH)_2$ (Table 2). Based on analysis of CEC, Na^+ was the main

interlayer cation of saponite, and the CEC of saponite was 130.7 ± 5.3 meq/100 g (Table S2). After saturated by Mg^{2+} , (001) reflection of saponite expanded to 14.9 Å ($5.9^\circ 2\theta$) (Fig. 3a), and saponite is known to contain two layers of interlayer H_2O in this case (Paterson and Swaffield, 1987). On the other hand, TGA-DSC results showed a large weight loss ($\sim 20\%$) and two endothermic peaks at

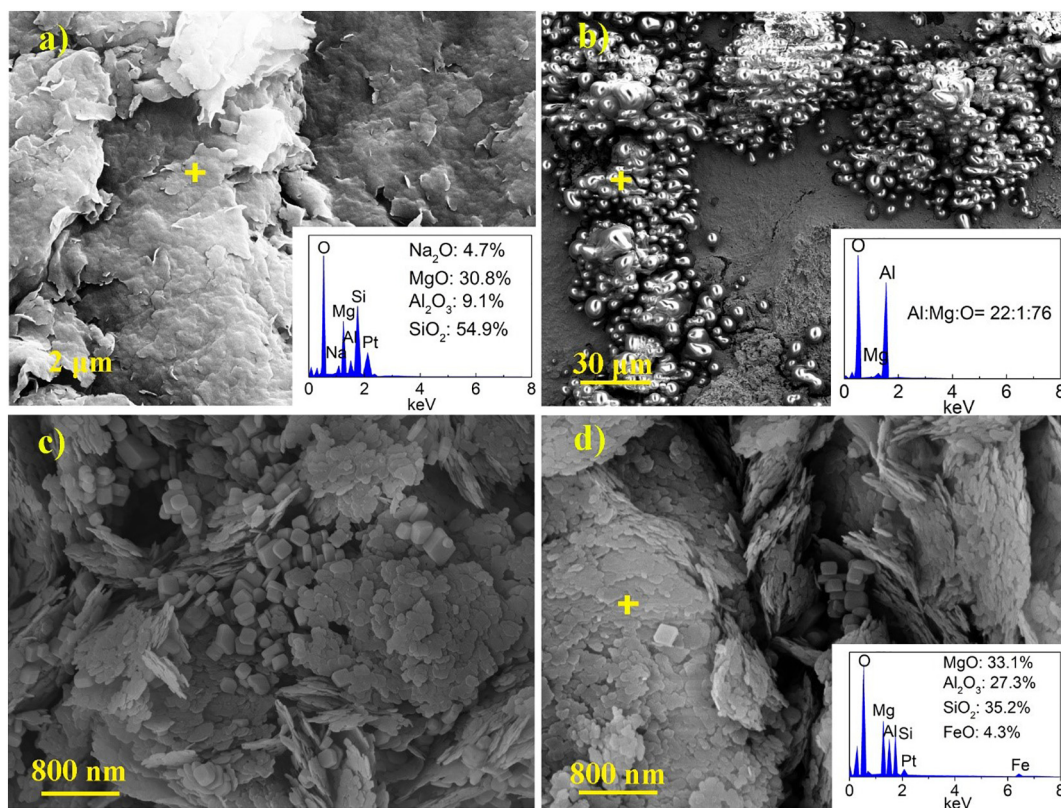


Fig. 4. Example SEM images and EDX spectra of saponite and solid products. a) saponite; b) amorphous materials at the beginning of reaction (III-0.33h); c) presence of boehmite in II-24h; d) chlorite in III-24h. Yellow cross indicates the location for EDX analysis. (For interpretation of the references to colour in this figure legend, the reader is referred to the web version of this article.)

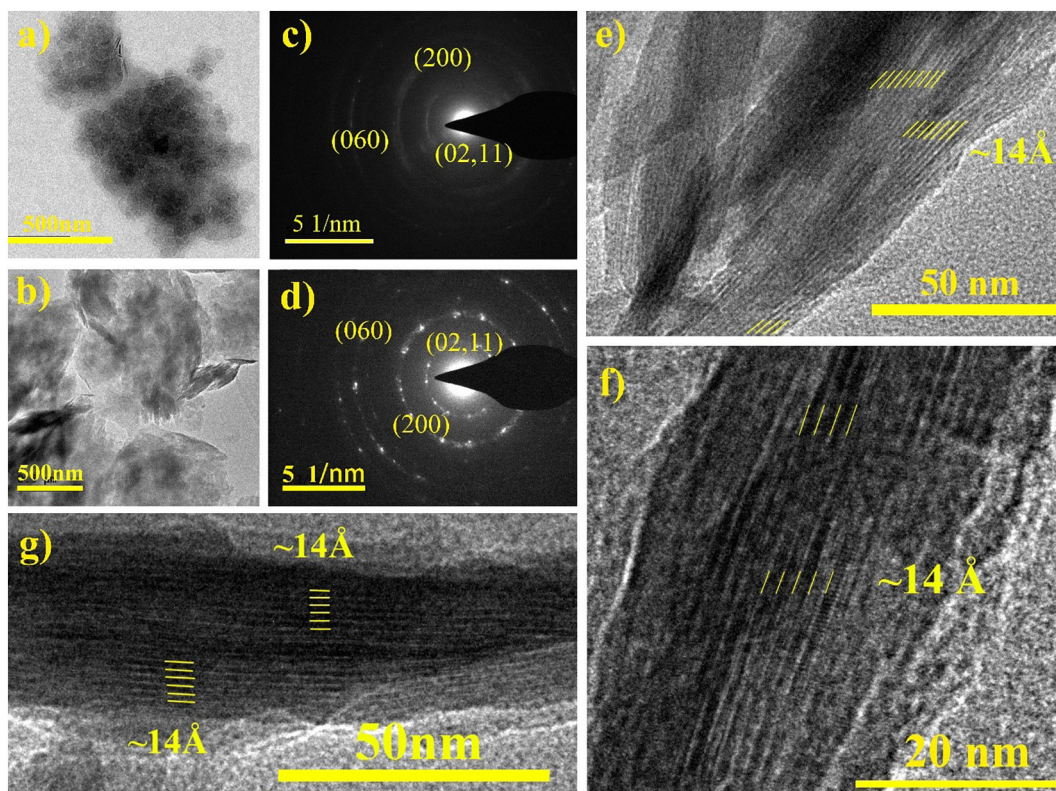


Fig. 5. TEM analysis of chlorite from (a) Series I at 24 h (I-24h) and (b) Series III at 24 h (III-24h). (c) and (d) are SAED images of I-24h and III-24h, respectively; (e), (f), and (d) show the 00*l* lattice fringes of chlorite, with the yellow numbers indicating average layer distance measured by TEM. (For interpretation of the references to colour in this figure legend, the reader is referred to the web version of this article.)

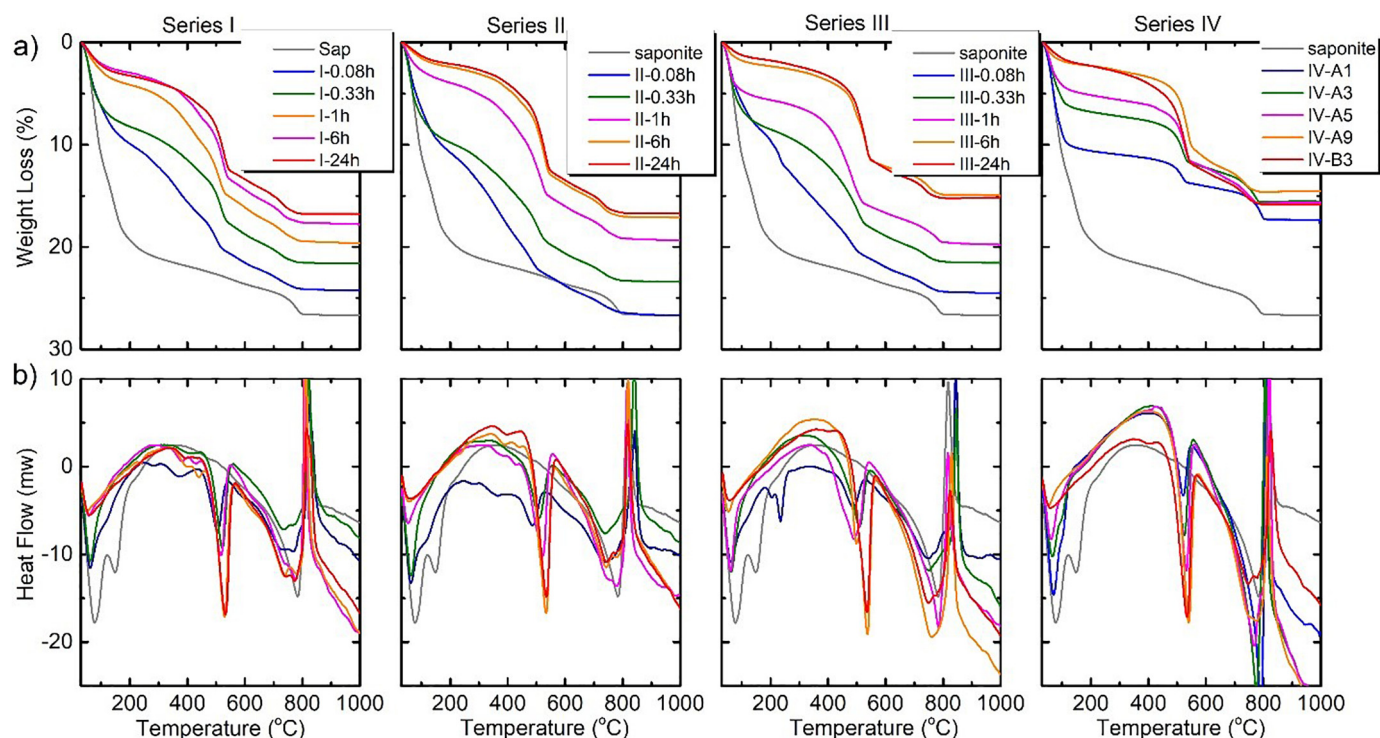


Fig. 6. (a) TGA and (b) DSC measurements of saponite after Mg^{2+} saturation and solid products from Series I-IV.

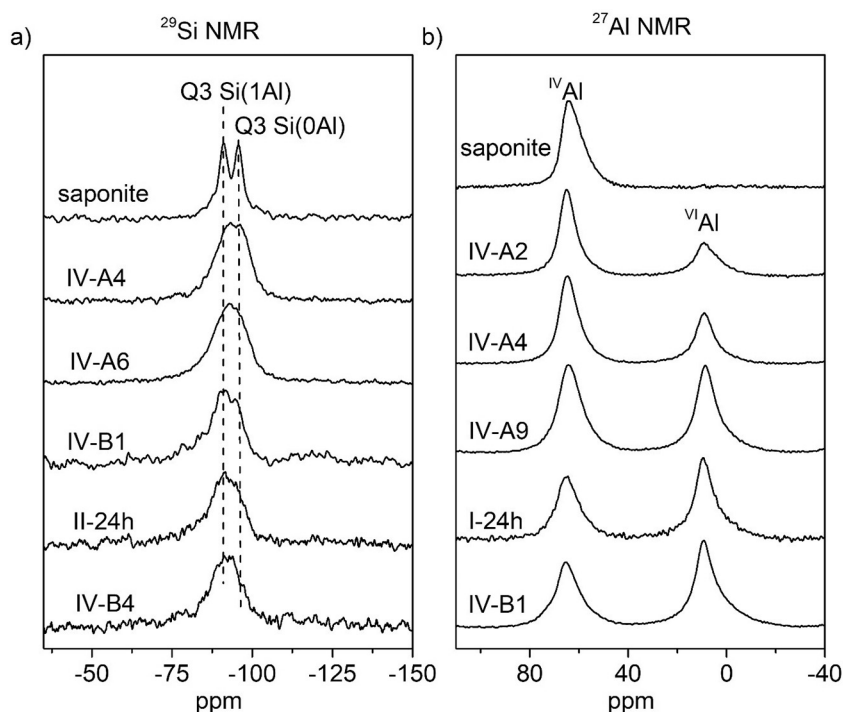


Fig. 7. (a) ^{29}Si and (b) ^{27}Al MAS NMR spectra of saponite and solid products from Series I–IV. Samples from top to bottom were listed with increasing Al^{3+} supply. $^{\text{IV}}\text{Al}$ denotes Al at tetrahedral sites, and $^{\text{VI}}\text{Al}$ represents Al at octahedral sites.

temperature < 200 °C due to loss of two-layered interlayer H_2O (Fig. 6).

3.2. Reaction processes of S–C conversion

3.2.1. Evolution of solution phase

pH changes and cation concentrations of the solution phases in Series I–III were plotted in Fig. 1. In the first 6 h, pH quickly decreased by 1–2 units, and then gradually approached steady state over 24 h (Fig. 1a). The final pH was around 7.6 in Series I, 7.0 in Series II, and 6.5 in Series III. Meanwhile, Mg concentration decreased from 20 mM to 10–5 mM for all series, while Al concentration was typically < 0.5 mM during the whole reaction (Fig. 1b and Table S3).

3.2.2. Evolution of solid products

Oriented XRD patterns of the air-dried solid products and saponite were shown in Fig. 2. Compared to saponite, the solid products from Series I–III displayed distinct XRD patterns with small reflections at ~ 5.9 , 12.2 , 18.4 , 24.5 , and $30.9^\circ 2\theta$ and corresponding d values at around 15, 7.2, 4.8, 3.6, and 2.88 \AA , respectively. These reflections gradually increased in intensity and shifted to lower d-spacing (e.g., 15 to 14.4 \AA) as reaction proceeded, steadily showing a XRD pattern similar to chlorite. Oriented XRD patterns of the solid products after different treatments were plotted in Fig. 3. Unlike saponite, the (001) reflection of the solid products from Series I–III barely changed position after EG-salvation, and only slightly collapsed to 13.9 \AA ($6.4^\circ 2\theta$) after heat treatment at 350 °C. After 24 h, the (001) reflection persisted at 14.4 \AA ($6.1^\circ 2\theta$) after EG-salvation and heat treatment at 350 °C, and only collapsed to 13.9 \AA ($6.4^\circ 2\theta$) after heat treatment at 550 °C (Fig. 3). Such properties clearly indicated formation of chlorite after 24 h (Moore and Reynolds, 1989).

Based on EDX analysis, the synthesized chlorite at 24 h was more enriched in MgO and Al_2O_3 and depleted in Na_2O and SiO_2 than saponite (Fig. 4d and Table S1). There was a minor increase of Fe (as FeO) in the synthesized chlorite, which probably was from the hydrothermal reactors due to corrosion at high temperature (Table S3). The FeO content (wt%) in all solid products, however, was well below 5% (Table

S1).

Selected solid products (I-24h and III-24h) were further examined by TEM to confirm the formation of chlorite from saponite (Fig. 5). The SAED patterns recorded normal to clay layers showed clear ($hk0$) reflections with calculated lattice distance at 4.60, 2.61, and 1.54 \AA , which are consistent with the (02,11), (200), and (060) reflections of chlorite, respectively (Figs. 5c and d) (Bailey, 1988; Brown and Bailey, 1962). The discrete reflection spots with different intensities in Fig. 5d were likely due to small coherent domains poorly extended along c^* . On the other hand, (00l) lattice fringes with layer spacing of $\sim 14 \text{ \AA}$ were extensively observed (Figs. 5e, f, and g), while no “saponite-like” layers were present, i.e., 10 \AA layer spacing due to collapse in high vacuum environment (Robinson and De Zamora, 1999). Thus, chlorite was successfully synthesized from saponite over 24 h.

There are other phases observed during S–C conversion. Reflections at 14.5 , 28.2 , and $38.4^\circ 2\theta$ (corresponding d values at 6.1, 3.16, and 2.35 \AA) indicated the presence of boehmite (AlOOH) (Fig. 2). Based on the intensity of its reflections, boehmite was negligible in Series I but abundant in Series II and III. During reaction, boehmite first appeared at 1 h, and continuously decreased in amount with reaction proceeding (Fig. 2). Observed by SEM, plenty of cubic particles with particle size of 200 nm distributed among flaky chlorite particles (Fig. 4c). They might be boehmite particles as shown by XRD. Additionally, considerable amounts of spherical materials were present at the beginning of reaction (Fig. 4b), which were mainly composed of Al and O. Since there were no reflections of this phase shown in XRD (Fig. 2), it might be an X-ray amorphous phase (e.g., amorphous Al-hydroxides). This amorphous phase disappeared quickly after 1 h of reaction and was not observed after 24 h (Fig. S1).

The solid products were characterized by CEC, TGA-DSC, and FTIR as well in order to trace the S–C conversion. The CEC of solid products at 0.08 h ($100\text{--}120 \text{ meq}/100 \text{ g}$) was similar to that of saponite, although Mg^{2+} became the main cation in interlayer (Table S2). The CEC of solid products gradually decreased from $120 \text{ meq}/100 \text{ g}$ to $20 \text{ meq}/100 \text{ g}$ over 24 h (Fig. 1c). At the same time, TGA-DSC measurements showed that the weight loss from dehydration and the intensity of corresponding endothermic peak at temperature < 200 °C continuously

decreased as reaction proceeded (Fig. 6). On the other hand, a new weight loss and endothermic peak developed at 450–550 °C, which were likely from dehydroxylation of hydroxide layers (Paterson and Swaffield, 1987). Thus, the original interlayer of saponite with H₂O and cations was gradually occupied by newly-formed hydroxide layers during S–C conversion. As for the FTIR, its results were consistent with other complementary techniques. Therefore, FTIR results were detailed in Text S1 and Figs. S2 and S3 to avoid redundancy.

3.3. Influence of Mg²⁺ and Al³⁺ supplies on S–C conversion

A variety of solid products was obtained in Series IV. With increasing Mg²⁺ and Al³⁺ supplies but a constant Mg/Al ratio (IV-A1 to IV-A9), the (001) reflection of the air-dried solid products progressively increased from 13.9 Å (6.4°2θ) to 14.4 Å (6.1°2θ), while the (001) reflection after EG solvation gradually decreased from 16.8 Å (5.3°2θ) to 14.4 Å (6.1°2θ) (Figs. 3e and S4). TGA-DSC results showed growing amounts of hydroxide layers and decreasing interlayer H₂O from IV-A1 to IV-A9 (Fig. 6), and meanwhile, the CEC declined continuously (Table S2). These properties suggested that the solid products from IV-A1 to IV-A9 were randomly mixed-layered C/S (Moore and Reynolds, 1989). Based on the (001) reflection position after EG-solvation (Reynolds, 1980), the percentage of chlorite (%C) in IV-A1 to IV-A9 were estimated to progressively increase from 10 to 84% (Table 1). However, corrensite, the regularly mixed-layered C/S (with diagnostic superlattice at around 29 Å (3.0°2θ)) was not observed.

Based on XRD, the solid products in IV-B1 to B5 were chlorite with or without boehmite, and the amount of boehmite increased with decreasing Mg/Al ratios (Figs. 2 and S5). With systematic changes of Mg/Al ratios, the chemical composition of synthesized chlorite of I-24h, II-24h, III-24h, and IV-B1 to IV-B5 altered as well. Formulae of chlorite were calculated on the scale of O₁₀(OH)₈ and reported in Table 2. Compared to saponite, the amounts of Al at tetrahedral sites (^{IV}Al) and octahedral sites (^{VI}Al) and Mg at octahedral sites of chlorite were found to increase after S–C conversion. The increase of ^{VI}Al and Mg at octahedral sites was due to formation of hydroxide layers, while the increasing ^{IV}Al suggested substitution of Al for Si in 2:1 layers.

In order to cross-validate the increasing ^{IV}Al and ^{VI}Al during S–C conversion, ²⁹Si and ²⁷Al MAS NMR spectra were collected (Fig. 7). For the ²⁹Si NMR spectra (Fig. 7a), saponite displayed two well-resolved peaks centered at –95 and –91 ppm, corresponding to Q³ Si(OAl) and Q³ Si(1Al), respectively (He et al., 2014). With increasing Al³⁺ supply, the Q³ Si(1Al) signal of solid products became more dominant, while Q³ Si(OAl) signal became a shoulder (Fig. 7a), suggesting an increasing amount of ^{IV}Al via substitution of Al for Si (He et al., 2014). On the other hand, a single peak at around 65 ppm was recorded in the ²⁷Al NMR spectrum of saponite (Fig. 7b), corresponding to ^{IV}Al in 2:1 layers (He et al., 2017). With increasing Al³⁺ supply, another peak gradually developed at around 9 ppm, which arose from the ^{VI}Al (Tao et al., 2018). This peak intensity continuously increased compared to ^{IV}Al, confirming the increasing ^{VI}Al during S–C conversion.

Control experiments were also conducted to better constrain the mechanisms of S–C conversion. The XRD pattern of the blank (IV-C1) showed a strong (001) reflection at 13.0 Å (6.8°2θ) (Fig. 2d), and after EG solvation, (001) reflection expanded to 17.0 Å (5.2°2θ) (Fig. S5). Thus, the blank was mixed-layered C/S and the C% was estimated to be 3%. Similarly, the Al-free control (IV-C2) was also identified as mixed-layered C/S and the C% was about 20% (Figs. 2d and S5). The Mg-free control (IV-C3), however, contained phases with a series of reflections at 7.0, 9.0, 12.4, 25.4, and 27.8°2θ (corresponding d values at 12.6, 9.8, 7.1, 3.5, and 3.2 Å), which were not identified (Fig. 2d). Nevertheless, there were no reflections indicating formation of mixed-layered C/S or chlorite.

4. Mechanisms of S–C conversion and effects of Mg²⁺ and Al³⁺ supplies

4.1. Mechanisms of S–C conversion: solid-state transformation

Two mechanisms have been invoked to explain the S–C conversion (Beaufort et al., 2015). Solid-state transformation (SST) mechanism assumes that chloritic layers are formed by alteration of smectite interlayer, along with necessary modification of surrounding portion of layers (Bettison-Varga and MacKinnon, 1997; Inoue et al., 1984). Dissolution-crystallization (DC) mechanism describes dissolution of smectite followed by nucleation and growth of chloritic layers in response to prevailing chemistry conditions (Meunier et al., 1991).

The S–C conversion in this study likely took place through SST based on the following reasons. Firstly, occurrence of DC would presumably result in, for example, increasing Mg²⁺ concentration from saponite dissolution, followed by a gradual decrease of Mg²⁺ due to formation of chlorite. However, Mg²⁺ concentration continuously decreased from 20 to 5 mM in Series I–III, along with progressive decrease of pH by 1.5–3 units throughout the reaction (Fig. 1). These features argued against the occurrence of DC. Secondly, the blank (IV-C1) was identified as mixed-layered C/S with only 3% chloritic layers (Figs. 2d and S5). Such a result suggested that the dissolution of saponite did occur under the experimental condition but was not significant in the short-term experiments (72 h). Previous studies also proposed that SST was the dominant mechanism in short-duration experiments (Meng et al., 2018; Mosser-Ruck et al., 2016). Therefore, the SST was, at least, the dominant mechanism in this study.

4.2. Mechanisms of S–C conversion: formation of hydroxide layers

The XRD patterns of the solid products at 0.08 h from Series I–III were totally different from that of saponite: the (001) reflection shifted from 12.6 to 15.0 Å and its intensity sharply decreased (Fig. 2). This alteration can be explained by the formation of incomplete hydroxide layers or island-like Mg–Al polymers in interlayer. Mg–Al polymers were commonly found in the interlayer of natural smectite and vermiculite (Barnhisel and Bertsch, 1989). The presence of Mg–Al polymeric islands can strongly modify the expansion or collapse properties, leading to minor shift of (001) reflection after heat treatment and EG-solvation (Meunier, 2007), as observed in Series I–III (Fig. 3). Meanwhile, because the hydroxide layers were incomplete, interlayer H₂O coexisted with hydroxide layers, resulting in weight loss both from dehydration and dehydroxylation (Fig. 6).

Incomplete hydroxide layers or Mg–Al polymers tend to form more complete hydroxide layers through polymerization (Meunier, 2007; Meunier et al., 1991) (Fig. 8). Based on TGA-DSC results, the endothermic peak of dehydroxylation increased as reaction proceeded in Series I–III (Fig. 6), suggesting the growth of hydroxide layers. The exact process of polymerization in interlayer remained unknown. Possible pathways might include migration of polymers in interlayer, formation of chemical bonds, and rejection of impurities (Meunier, 2007). In Series I–III, amorphous Al-hydroxide disappeared (Fig. S1) and boehmite decreased in amount during reaction (Fig. 2), which processes might continuously provide Al³⁺ for the formation of hydroxide layers. Mg²⁺ in solution, on the other hand, might be consumed by the polymerization process, leading to decreasing amount of Mg²⁺ (Fig. 1b). Thus, formation of hydroxide layers would directly depend on the availability of Mg–Al polymers. This might explain the successful formation of chlorite when Mg²⁺ and Al³⁺ were abundant (Series I–III and IV-B1 to B5) and the yield of mixed-layered C/S when Mg²⁺ and Al³⁺ were limited (IV-A1 to IV-A9) or absent (the blank of IV-C1).

4.3. Mechanisms of S–C conversion: substitution of Al for Si in 2:1 layers

In the Al-free control (IV-C2), although Mg²⁺ was abundant

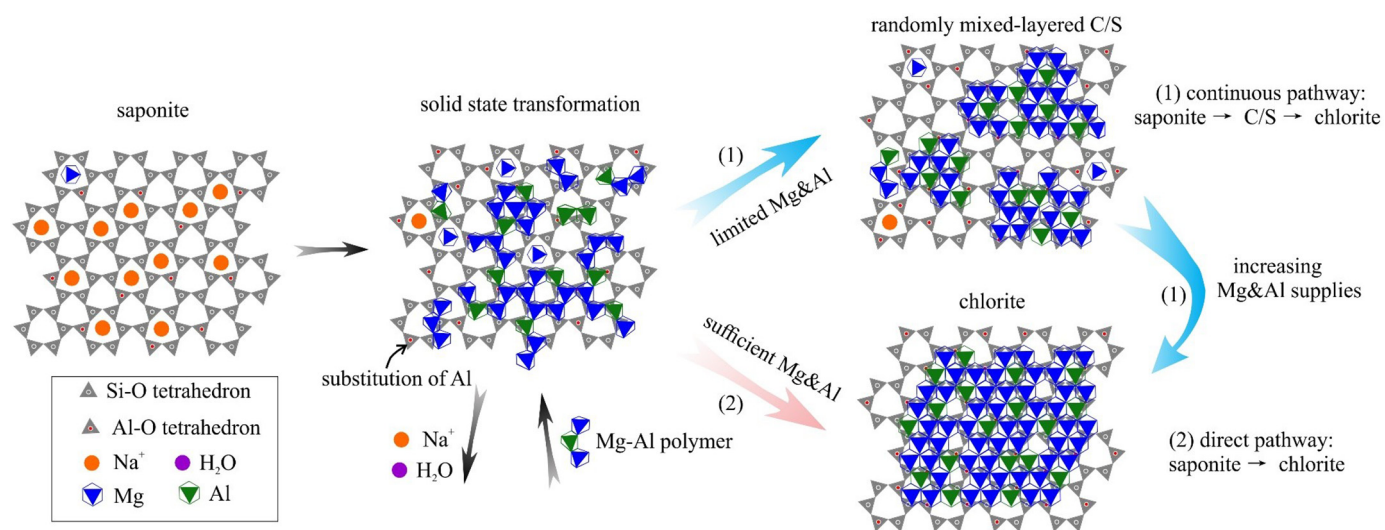


Fig. 8. Schematic figure showing the proposed solid-state transformation of smectite to chlorite. Mg–Al polymers replace Na^+ and H_2O in the interlayer of saponite, and gradually form hydroxide layers through polymerization, coupling with substitution of Al^{3+} for Si^{4+} in the 2:1 layers. When Mg^{2+} and Al^{3+} are limited, mixed-layered C/S would form from saponite, and growing Mg^{2+} and Al^{3+} supplies would continuously increase the percentage of chlorite in mixed-layered C/S until chlorite form (saponite \rightarrow mixed-layered C/S \rightarrow chlorite). In contrast, chlorite could form directly from saponite under sufficient Mg^{2+} and Al^{3+} supplies (saponite \rightarrow chlorite).

(185 mM), saponite only transformed to mixed-layered C/S with 20% chloritic layers. The combined NMR (Fig. 7) and chlorite formula calculation (Table 2) showed increasing substitution of Al for Si in 2:1 layers during S–C conversion. These observations might indicate critical roles of Al substitution for Si in S–C conversion (Fig. 8). The roles might include (1) reducing crystallographic constraints between saponite and chlorite and (2) enhancing formation of hydroxide layers from Mg–Al polymers. The *b*-dimension of chlorite (9.25–9.30 Å, Bailey, 1988) is slightly larger than that of saponite (9.23 Å, Suquet et al., 1975), which might hinder the S–C conversion (Meunier et al., 1991). However, this crystallographic constraint would be reduced by substitution of larger Al^{3+} (ionic radius 0.39 Å) for Si^{4+} (0.26 Å) (Suquet et al., 1981). Secondly, increasing substitution of Al for Si resulted in more negatively charged 2:1 layers, which would facilitate the fixation and polymerization of Mg–Al polymers. Al-polymers were suggested to be more retained in interlayer with increasing layer charge (Hsu, 1992). Our results also showed that, for Al-free control (IV-C2), 147 mM Mg^{2+} out of 185 mM initial Mg^{2+} supply remained in solution after reaction, instead of being fixed in interlayer (Table S3).

4.4. Mg^{2+} and Al^{3+} supplies determining S–C conversion models

This study succeeded in hydrothermal synthesis of chlorite from saponite, and for the first time, it experimentally demonstrated that either randomly mixed-layered C/S or chlorite could form from saponite depending on the availability of Mg^{2+} and Al^{3+} (Fig. 8). When Mg^{2+} and Al^{3+} were limited, mixed-layered C/S would form from saponite, and growing Mg^{2+} and Al^{3+} supplies would progressively increase the C% in mixed-layered C/S until chlorite formed (IV-A1 to IV-A9). This case corresponded to the continuous model introduced previously. In contrast, chlorite could form directly from saponite without presence of mixed-layered C/S under sufficient Mg^{2+} and Al^{3+} supplies (Series I–III and IV-B1 to IV-B5), which corresponded to the direct model.

Thus, we hypothesize that the long-standing debate on the S–C conversion models (continuous vs. direct) could be solved by considering the availability of elements. In natural environments, pore water and dissolution of Mg- or Al-containing minerals (e.g., dolomite and feldspar) are possible sources of Mg and Al for S–C conversion. The availability of Mg and Al, thus, would be closely associated with the intensity of fluid/rock interaction. Fluid/rock interaction has been

regarded as the controlling factor in regulating S–C conversion pathways in previous studies (e.g., Robinson and De Zamora, 1999; Schiffman and Staudigel, 1995; Shau and Peacor, 1992; Shau et al., 1990). For example, in the Chipilapa (El Salvador), direct conversion of smectite into chlorite with rare occurrence of mixed-layered C/S or corrensite was observed (Robinson and De Zamora, 1999; Robinson et al., 2002). This geothermal system was typical of high fluid/rock interaction, characterized with extensive secondary mineralization and high permeability (Robinson and De Zamora, 1999). In marked contrast, randomly mixed-layered C/S might form in micro-environments under lower fluid/rock ratio with insufficient element supplies (Bettison-Varga and MacKinnon, 1997). Thus, sufficient, time-integrated supplies of critical elements for S–C conversion due to high fluid/rock interaction might give rise to the direct formation of chlorite, while limited nutrient supplies would result in the presence of randomly mixed-layered C/S (Beaufort et al., 2015; Robinson et al., 2002).

The discontinuous model was not observed in this study, which involves formation of corrensite. Corrensite has been suggested to be better regarded as a unique phase rather than regularly mixed-layered C/S due to its distinct crystallographic properties of stacking sequence and the distribution of Fe, Mg, and layer charges (Beaufort et al., 1997; Murakami et al., 1999; Shau et al., 1990). Because of above difference, corrensite was suggested to form from smectite through DC, rather than SST (Inoue et al., 1984; Roberson et al., 1999). Since SST was the dominant mechanism of S–C conversion in this study, the absence of corrensite, in return, likely suggested that corrensite might only form from smectite via DC.

Finally, it is worth to noting that the hydrothermal temperature in this study (340 °C) was slightly higher than the commonly observed temperature range of chlorite in natural environments (200–300 °C) (Beaufort et al., 2015), and in addition to temperature, other parameters (e.g., fluid/rock ratio and pH) might also influence the S–C conversion to some degrees (Robinson et al., 2002). The current study focused on the kinetics and mechanisms of S–C conversion and only examined the influence of Mg–Al supplies on S–C conversion pathways with no examination on other experimental parameters (e.g., temperature, fluid/rock ratio, and pH). However, further studies could be conducted to examine the effects of each parameter using the hydrothermal method established in this study, in order to further constrain the S–C conversion under environmentally relevant conditions and

explore potential applications of this common clay transformation reaction.

5. Conclusions

S–C conversion is an important reaction of clay mineral transformations, but current models and mechanisms of S–C conversion are still under debate. In this study, saponite was reacted with Mg^{2+} and Al^{3+} in NaCl solution at 340 °C, autogenous pressure, liquid/solid ratio of 30, and initial pH of 9.0. Reaction products were characterized by ICP-OES, XRD, TGA-DSC, SEM-EDX, TEM, FTIR, and NMR. The results showed:

- (1) saponite could transform to mixed-layered C/S or chlorite via SST at 24 h;
- (2) Mg^{2+} and Al^{3+} supplies are important for formation of hydroxide layers, and the concomitant substitution of Al for Si might play important roles in driving S–C conversion;
- (3) the formation of mixed-layered C/S or chlorite depended on Mg^{2+} and Al^{3+} supplies. When Mg^{2+} and Al^{3+} were limited, mixed-layered C/S would form from saponite, and growing Mg^{2+} and Al^{3+} supplies would continuously increase the percentage of chlorite in mixed-layered C/S until chlorite formed (saponite → mixed-layered C/S → chlorite). In marked contrast, chlorite could form directly from saponite under sufficient Mg^{2+} and Al^{3+} supplies (saponite → chlorite).

This study contributed to an improved understanding of the S–C conversion mechanisms and roles of Mg^{2+} and Al^{3+} supplies in determining S–C conversion pathways, and provided a general methodology and knowledge basis for future studies on this mineral conversion.

Declaration of competing interest

The authors declare that they have no known competing financial interests or personal relationships that could have appeared to influence the work reported in this paper.

Acknowledgement

This work is supported by the National Natural Science Foundation of China (NSFC) (Grant No. 41672115 and 41673095) and Major Project of National Petroleum in China (Grant No. 2016ZX05006-001-003). YT acknowledges funding support from US National Science Foundation (NSF) under grant numbers 1605692 and 1739884. The authors appreciate comments and suggestions from the reviewers and editor. The authors acknowledge Wanyi Lu, Tong He, Xianqiang Meng (Nanjing University, Nanjing, China), and Rixiang Huang (Georgia Institute of Technology, Atlanta, USA) for instrumental support and data interpretation.

Appendix A. Supplementary data

Supplementary data to this article can be found online at <https://doi.org/10.1016/j.clay.2019.105357>.

References

April, R.H., 1981. Trioctahedral smectite and interstratified chlorite/smectite in Jurassic strata of the Connecticut Valley. *Clay Clay Miner.* 29, 31–39.

Bailey, S., 1988. X-ray diffraction identification of the polytypes of mica, serpentine, and chlorite. *Clay Clay Miner.* 36, 193–213.

Barnhisel, R.I., Bertsch, P.M., 1989. Chlorites and hydroxy-interlayered vermiculite and smectite. *Miner. Soil Environ.* 729–788.

Beaufort, D., Baronnet, A., Lanson, B., Meunier, A., 1997. Corrensite: a single phase or a mixed-layer phyllosilicate in the saponite-to-chlorite conversion series? A case study of Sancerre-Couy deep drill hole (France). *Am. Mineral.* 82, 109–124.

Beaufort, D., Rigault, C., Billon, S., Billault, V., Inoue, A., Inoue, S., Patrier, P., 2015. Chlorite and chloritization processes through mixed-layer mineral series in low-temperature geological systems—a review. *Clay Miner.* 50, 497–523.

Bettison, L.A., Schiffman, P., 1988. Compositional and structural variations of phyllosilicates from the Point Sal ophiolite, California. *Am. Mineral.* 73, 62–76.

Bettison-Varga, L., MacKinnon, I.D., 1997. The role of randomly mixed-layered chlorite/smectite in the transformation of smectite to chlorite. *Clay Clay Miner.* 45, 506–516.

Brown, B.T., Bailey, S., 1962. Chlorite polytypism: I. Regular and semi-random one-layer structures. *Am. Mineral. J. Earth Planet. Mater.* 47, 819–850.

Chang, H.K., Mackenzie, F.T., Schoonmaker, J., 1986. Comparisons between the diagenesis of dioctahedral and trioctahedral smectite, Brazilian offshore basins. *Clay Clay Miner.* 34, 407–423.

Chapman, H., 1965. Cation-exchange capacity 1. Methods of soil analysis. Part 2. *Chem. Microbiol. Prop.* 891–901.

Dowey, P.J., Hodgson, D.M., Worden, R.H., 2012. Pre-requisites, processes, and prediction of chlorite grain coatings in petroleum reservoirs: a review of subsurface examples. *Mar. Pet. Geol.* 32, 63–75.

Guillaume, D., Neaman, A., Cathelineau, M., Mosser-Ruck, R., Peiffert, C., Abdelmoula, M., Dubessy, J., Villiéras, F., Baronnet, A., Michau, N., 2003. Experimental synthesis of chlorite from smectite at 300 °C in the presence of metallic Fe. *Clay Miner.* 38, 281–302.

He, H., Li, T., Tao, Q., Chen, T., Zhang, D., Zhu, J., Yuan, P., Zhu, R., 2014. Aluminum ion occupancy in the structure of synthetic saponites: effect on crystallinity. *Am. Mineral.* 99, 109–116.

He, H., Ji, S., Tao, Q., Zhu, J., Chen, T., Liang, X., Li, Z., Dong, H., 2017. Transformation of halloysite and kaolinite into beidellite under hydrothermal condition. *Am. Mineral.* 102, 997–1005.

Hsu, P.H., 1992. Reaction of OH-Al polymers with smectites and vermiculites. *Clay Clay Miner.* 40, 300–305.

Inoue, A., Utada, M., 1991. Smectite-to-chlorite transformation in thermally metamorphosed volcanoclastic rocks in the Kamikita area, northern Honshu, Japan. *Am. Mineral.* 76, 628–640.

Inoue, A., Utada, M., Nagata, H., Watanabe, T., 1984. Conversion of trioctahedral smectite to interstratified chlorite/smectite in Pliocene acidic pyroclastic sediments of the Ohyu district, Akita Prefecture, Japan. *Clay Sci.* 6, 103–116.

Meng, J., Liu, X., Li, B., Zhang, J., Hu, D., Chen, J., Shi, W., 2018. Conversion reactions from dioctahedral smectite to trioctahedral chlorite and their structural simulations. *Appl. Clay Sci.* 158, 252–263.

Meunier, A., 2007. Soil hydroxy-interlayered minerals: a re-interpretation of their crystallochemical properties. *Clay Clay Miner.* 55, 380–388.

Meunier, A., Inoue, A., Beaufort, D., 1991. Chemiographic analysis of trioctahedral smectite-to-chlorite conversion series from the Ohyu Caldera, Japan. *Clay Clay Miner.* 39, 409–415.

Moore, D.M., Reynolds, R.C., 1989. X-Ray Diffraction and the Identification and Analysis of Clay Minerals. Oxford University Press, New York.

Mosser-Ruck, R., Pironon, J., Guillaume, D., Cathelineau, M., 2003. Experimental alteration of Mg-vermiculite under hydrothermal conditions: formation of mixed-layered saponite-chlorite minerals. *Clay Miner.* 38, 303–314.

Mosser-Ruck, R., Cathelineau, M., Guillaume, D., Charpentier, D., Rousset, D., Barres, O., Michau, N., 2010. Effects of temperature, pH, and iron/clay and liquid/clay ratios on experimental conversion of dioctahedral smectite to berthierine, chlorite, vermiculite, or saponite. *Clay Clay Miner.* 58, 280–291.

Mosser-Ruck, R., Pignatelli, I., Bourdelle, F., Abdelmoula, M., Barres, O., Guillaume, D., Charpentier, D., Rousset, D., Cathelineau, M., Michau, N., 2016. Contribution of long-term hydrothermal experiments for understanding the smectite-to-chlorite conversion in geological environments. *Contrib. Mineral. Petrol.* 171, 97.

Murakami, T., Sato, T., Inoue, A., 1999. HRTEM evidence for the process and mechanism of saponite-to-chlorite conversion through corrensite. *Am. Mineral.* 84, 1080–1087.

Paterson, E., Swaffield, R., 1987. Thermal analysis. In: Wilson, M.J. (Ed.), *A Handbook of Determinative Methods in Clay Mineralogy*. Blackie-Son Ltd., London, pp. 99–132.

Reynolds, R., 1980. Interstratified clay minerals. In: *Crystal Structures of Clay Minerals and their X-Ray Identification*, pp. 249–303.

Roberson, H.E., Reynolds, R.C., Jenkins, D.M., 1999. Hydrothermal synthesis of corrensite: a study of the transformation of saponite to corrensite. *Clay Clay Miner.* 47, 212–218.

Robinson, D., De Zamora, A.S., 1999. The smectite to chlorite transition in the Chipilapa geothermal system, El Salvador. *Am. Mineral.* 84, 607–619.

Robinson, D., Schmidt, S.T., Zamora, D., Santana, A., 2002. Reaction pathways and reaction progress for the smectite-to-chlorite transformation: evidence from hydrothermally altered metabasites. *J. Metamorph. Geol.* 20, 167–174.

Schiffman, P., Staudigel, H., 1995. The smectite to chlorite transition in a fossil seamount hydrothermal system: the basement complex of La Palma, Canary Islands. *J. Metamorph. Geol.* 13, 487–498.

Schleicher, A., van der Pluijm, B., Warr, L., 2012. Chlorite-smectite clay minerals and fault behavior: new evidence from the San Andreas Fault Observatory at Depth (SAFOD) core. *Lithosphere* 4, 209–220.

Shau, Y.-H., Peacor, D.R., 1992. Phyllosilicates in hydrothermally altered basalts from DSDP Hole 504B, Leg 83—a TEM and AEM study. *Contrib. Mineral. Petrol.* 112, 119–133.

Shau, Y.-H., Peacor, D.R., Essene, E.J., 1990. Corrensite and mixed-layer chlorite/corrensite in metabasalt from northern Taiwan: TEM/AEM, EMPA, XRD, and optical studies. *Contrib. Mineral. Petrol.* 105, 123–142.

Suquet, H., De La Calle, C., Pezerat, H., 1975. Swelling and structural organization of saponite. *Clay Clay Miner.* 23, 1–9.

Suquet, H., Malard, C., Copin, E., Pezerat, H., 1981. Variation du paramètre b et de la distance basale d 001 dans une série de saponites à charge croissante: I. Etats hydratés. *Clay Miner.* 16, 53–67.

Tao, Q., Chen, M., He, H., Komarneni, S., 2018. Hydrothermal transformation of mixed metal oxides and silicate anions to phyllosilicate under highly alkaline conditions. *Appl. Clay Sci.* 156, 224–230.